Research Article

Steady Wind Load on External Surface and Its Effect on Wind-Induced Response for a 200 m High Natural-Draught Cooling Tower

Yunfeng Zou,[1,2] Fanrong Xue,[1] Xuhui He,[1,2] Chenzhi Cai [1,2] and Shouke Li[3]

[1]*School of Civil Engineering, Central South University, Changsha, Hunan 410075, China*
[2]*Hunan Provincial Key Laboratory for Disaster Prevention and Mitigation of Rail Transit Engineering Structure, Changsha, Hunan 410075, China*
[3]*School of Civil Engineering, Hunan University of Science and Technology, Xiangtan, Hunan 411201, China*

Correspondence should be addressed to Chenzhi Cai; chenzhi.cai@csu.edu.cn

Wind tunnel tests were carried out to measure the wind pressure of a 200 m high natural-draught cooling tower. An analysis of the distribution characteristics of external pressure was then conducted to determine the pressure coefficients $Cp(\theta, z)$ in a given wind profile. Finally, the effect on the response of the shell and the buckling safety of the shell, applying the simplified height-constant pressure coefficient $Cp(\theta)$ and the realistic pressure $Cp(\theta, z)$, was determined. Taking the wind load specified in the code as an example, the influence of the distribution of external pressure on the wind-induced response was further analyzed. The results indicate that the pressure distribution varies with not only the height z but also the circumferential angle θ, and the wind load of both ends of the tower is significantly greater than that of its middle. Moreover, the wind-induced static responses of the tower under the action of the realistic pressure distribution $Cp(\theta, z)$ and the simplified approach $Cp(\theta)$ are basically consistent, because the wind load distribution is more important than its magnitude for the wind-induced response of cooling tower, and the wind-induced response of the cooling tower is dominated by the local shell deformation.

1. Introduction

Natural-draught cooling towers are high-rise and thin-walled flexible shell structures commonly used in thermal and nuclear power plants as cooling devices. The shell of a cooling tower is rather thin, and the ratio of the minimum shell thickness to the throat diameter is of the order of 1/400. In areas of negligible seismic activity, the dominating load of natural-draught cooling towers is induced by the action of turbulent wind due to the exposure of a large area to the wind (Bamu and Zingoni [1]; Nimeann and Zerna [2]; Hashish and Abu-Sitta [3]; Armitt [4]). In November 1965, three out of a group of eight reinforced-concrete cooling towers were blown down by strong wind at Ferrybridge Power Station in Yorkshire County in the UK (Central Electricity Generating Board, 1965) [5]. Since then, much

attention has been paid to the wind load and wind-induced response of cooling towers (Zou et al. [6]; Ke and Ge [7]; Ke et al. [8]; Zhao et al. [9]). Following Davenport's concept, the wind forces acting on the external surface of a cooling tower may be subdivided into mean forces (averaged over a period of some 10 minutes) and turbulent wind forces. Usually, the resonant response induced by turbulent wind forces is small and an appropriate gust response factor taking into account the effects of turbulence is used to determine a static design load (Zhang et al. [10]; Zou et al. [11]). An outline of the quasistatic wind action in cooling tower shells used in the current design practice was presented by Abu-Sitta and Hashish [12]. The effects of the wind load are usually determined by applying equivalent static loads in terms of surface pressures (Kasperski and Niemann [13]; Ke et al. [14]). Once quasistatic pressure distribution is defined, the

response to turbulent wind is introduced by the gust factors. Mean wind pressures are usually characterized by the pressure coefficients Cp.

$$Cp = \frac{p(\theta, z)}{q(z)}, \qquad (1)$$

where $p(\theta, z)$ is the mean wind pressure acting on the external surface of the shell depending on the circumferential angle θ and the height z above the ground level and $q(z)$ is the reference velocity pressure at height z.

As seen in equation (1), the pressure coefficients Cp depend on both the height z and the circumferential angle θ, $Cp = Cp(\theta, z)$, which is also confirmed by wind tunnel tests in shear flow. However, since the wind pressure distributions in various loading codes are based on data from on-the-spot measurements, in which sensors were usually installed at the area near the throat, and wind tunnel tests in homogeneous flow for cooling towers with heights of about 90 m~120 m (Sun and Zhou [15]; Sun et al. [16]), it has become common practice to use a simplified height-constant pressure distribution $Cp(\theta)$ in the current design, disregarding the fact that Cp values are height-dependent, and to attribute the influence of heights on the pressures to the wind profile alone. The wind pressure $p(\theta, z)$ at any point on the outer surface is then simplified as follows:

$$p(\theta, z) = Cp(\theta) \times q(z). \qquad (2)$$

However, with the rapid development of nuclear power plants on the mainland of China, a 200 m high natural-draught cooling tower has been proposed whose height would far exceed the 165 m height limit specified in the existing design codes for cooling towers in China (GB/T 50102 [17]; NDGJ5-88 [18]). Accordingly, the design value of the wind loading on the external surfaces of a cooling tower with a height of 200 m has attracted the extensive attention of Chinese engineers. The aim of the present study is to elaborate the differences between the simplified height-constant pressure distribution $Cp(\theta)$ and the realistic pressures $Cp(\theta, z)$ and to find out whether the design procedure is realistic or, at least, conservative. Firstly, the wind pressure coefficients on the external surface of a 200 m high natural-draught cooling tower are obtained by synchronous pressure measurements in wind tunnel tests in shear flow, which is a closer approximation of reality, to determine the pressure coefficients $Cp(\theta, z)$ in a given wind profile. Then, the resulting effect on the response of the shell and the buckling safety of the shell applying the simplified height-constant pressure coefficient $Cp(\theta)$ or the realistic pressure $Cp(\theta, z)$ was established. It should be noted that wind-induced interference effects in tower groups or from other adjacent buildings are not considered in the present study, so the results are restricted to the case of a single tower.

2. Details of Wind Tunnel Tests

2.1. Boundary Layer Wind Tunnel (BLWT) Configuration.

The wind tunnel test is conducted at the HD-2 BLWT at Hunan University, whose laboratory is a closed-circuit atmospheric boundary layer. The tests are carried out in turbulent shear flow in the high-speed test section (3.0 m in width and 2.5 m in height), and an artificial thickening of the boundary layer was achieved with the help of spires at the entrance and irregularities on the floor of the wind tunnel. The flow velocity was measured with a Cobra Probe, and the sampling time and sampling frequency were, respectively, set as 30 s and 2000 Hz. The duration of each sample was chosen to obtain an error of less than 0.5% on the mean value. The wind characteristics measured at the center of the rotary plate are shown in Figure 1. As shown in Figure 1(a), the mean wind speed profile is represented by the power law, and the profile exponent $\alpha = 0.16$, which corresponds to moderately rough terrain as specified in the Chinese loading code. The turbulence intensities at $z = 50$ cm and $z = 40$ cm above the floor are 15.6% and 16.6%, corresponding to the top and throat levels of the model tower, respectively. Figure 1(b) shows that the simulated longitudinal turbulence power spectrum at 50 cm above the floor is similar to common theoretical spectra, such as those generated by Von Kármán, Kaimal, and Davenport, which illustrates that the wind field simulation is reliable. In addition, the integral length scale is about 50 cm, corresponding to a full-scale value of 200 m.

2.2. Test Model. The total height of the prototype cooling tower is 200.00 m, the throat section above ground level is 156.70 m, and the inlet opening above ground level is 12.59 m, with a cooling area of 18,000 m^2. The diameters of the top, throat section, and bottom of the shell are 96.60 m, 94.60 m, and 153.00 m, respectively. The shell thickness varies with the height z. The minimum shell thickness (0.25 m) is at the throat section, whereas the maximum shell thickness (1.40 m) is at the lower stiffening ring, which is supported by 52 uniformly distributed pairs of Φ1.4 m V-shaped circular columns. The testing model was made from high-quality aluminum alloy by a digitally controlled lathe to ensure that the strength and stiffness of the model are sufficient and no deformation or obvious vibration occurs under the wind speed during the pressure measuring tests to guarantee the precision of the pressure measurements. The experimental model is geometrically similar to the prototype object, and the geometric scale ratio was chosen to be 1/400 (total height of the model $H = 0.5$ m). The maximum blockage ratio caused by the installation of the model is 4.6%, and thus its effects are neglected in the following discussions. The shell model was supported by 52 pairs of V-shaped circular column models, permitting the reproduction of the real draught. The photo of the processed model is given in Figure 2. A total of 20 levels of measurement points were arranged on the internal surface of the model, and 36 measurement points were placed at each level along the circumferential direction (i.e., an angular distance of 10°), resulting in 720 total pressure taps. Figure 3 presents the layout of the measurement points and the definition of the circumferential angle θ.
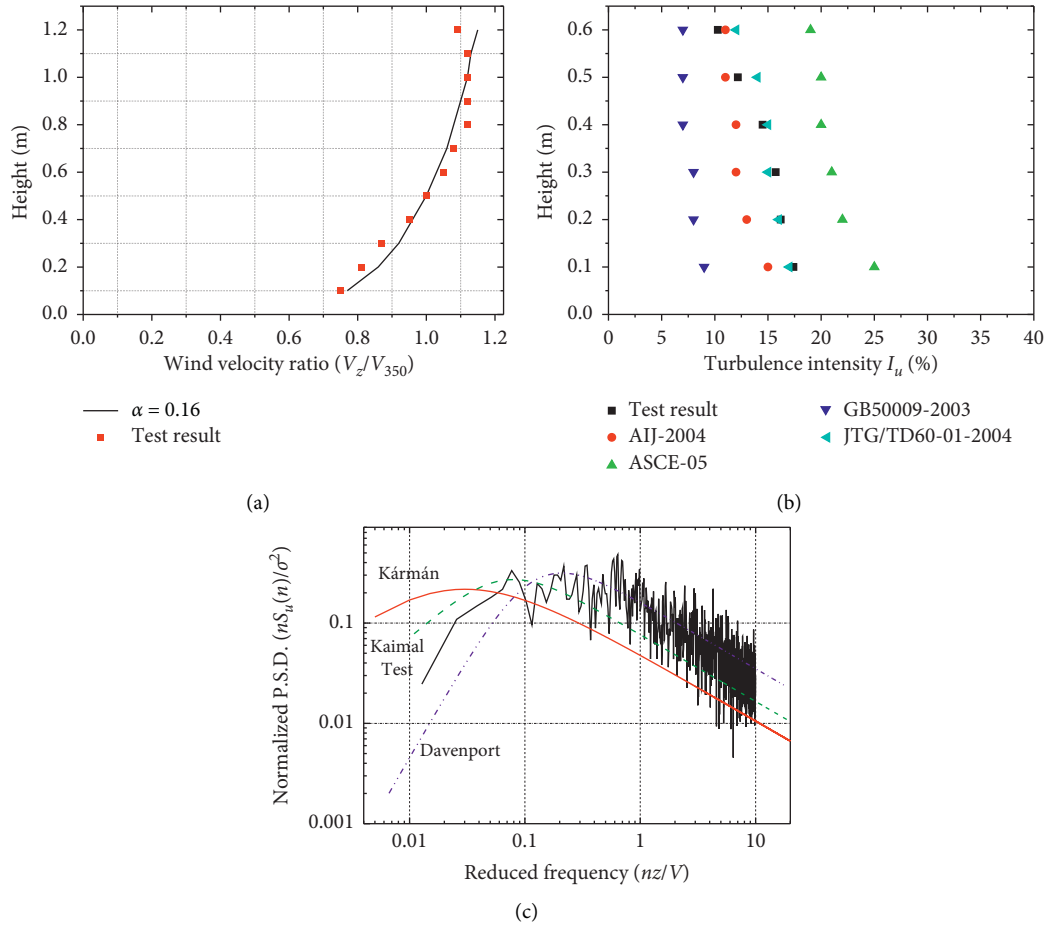
(a)

(b)

(c)

FIGURE 1: Simulation of wind characteristics in BLWT (V_z is the wind speed at height z, V350 is the gradient velocity, and I_u is the turbulent intensity). (a) Mean wind speed. (b) Turbulence intensity. (c) Longitudinal turbulence power spectrum.

2.3. Test Conditions. A DTC net electronic type pressure scanning system (Pressure Systems, Inc., USA) was employed to measure the wind pressure. In this study, sixteen modules were used and a total of 1024 pressure measuring points could be monitored simultaneously. The sampling duration of each measurement was 30 s and the sampling frequency was 330 Hz. The pressure taps were linked to the transducers with 500 mm silicon tubes with an inner diameter of 1.0 mm and an outer diameter of 2.0 mm. The system obtained had a flat amplitude and a linear variation of the phase up to the sampling frequency, which could guarantee the transmission of the fluctuations without distortions.

It is important to note that the flow conditions around rounded shapes are sensitive to the Reynolds number. However, the Reynolds number in a wind tunnel is usually 2~3 magnitudes less than that in full scale. Fortunately, the transcritical flow regime may be obtained by adding sufficient roughness to the model surface in the wind tunnel tests. It should be noted that the design curve is simulated by pasting a rough paper tape on the surface of the model to increase the surface roughness in the wind tunnel test, as shown in Figure 4. By making use of this beneficial effect, thirty-six equally spaced ribs 0.3 mm in height were applied

in the present study to provide an average roughness coefficient rib height to a distance of 0.015. In a preliminary test, it was found that the pressure distribution was unaffected for wind speeds V_H from 12 to 20 m/s. This was monitored using a Pitot tube at the centerline of the test section, about 3 m upstream of the tested model. The test results obtained at the free stream oncoming velocity $V_H = 18$ m/s were taken as representative, corresponding to a Reynolds number of 6.03×10^5 based on V_H and the mean diameter of the tower model.

2.4. Test Results of Mean Wind Load. To enable the data obtained from the wind tunnel tests to be applied to the prototypes, the pressure coefficients presented in this study are nondimensionalized, referring the pressures at a given height z to the velocity pressure $q(z)$ at the same height, as shown in equation (1). A positive pressure indicates the direction of the pressure force points into the surface of the structure, while a negative one indicates the direction points outwards from the surface. Since the cooling tower is axially symmetrical and the theoretical mean wind pressure distribution on the external surface should be symmetrical compared with the incoming wind direction, only half of the wind pressures (0° to 180°) are presented in this paper.

FIGURE 2: Test model.
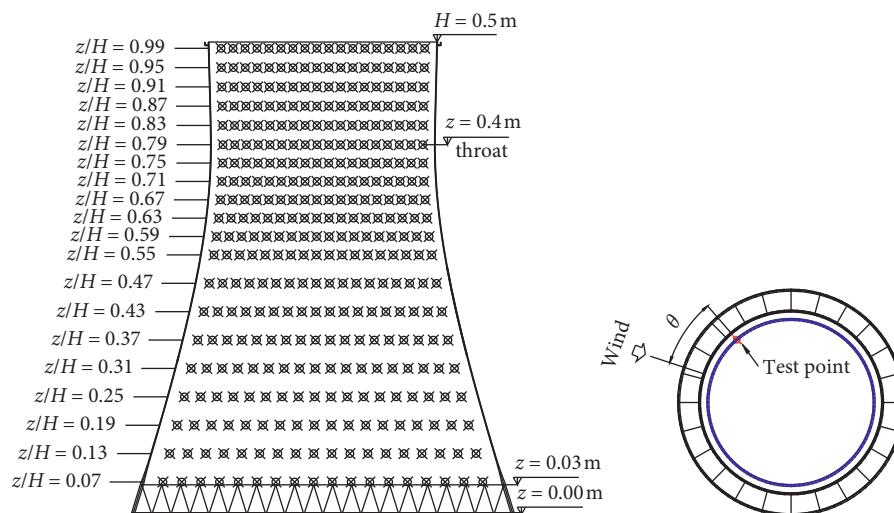
FIGURE 3: Pressure taps arrangement and the definition of θ.

The mean wind pressure coefficients at typical levels z/H measured at the free stream oncoming velocity $V_H = 18$ m/s are shown in Figure 5. It should be noted that the "typical curve" is the average of the pressure coefficients over the region $z/H = 0.30$ to 0.80, since the pressure distribution at this region is more or less independent of the height z. This is

in accordance with the data reported by Sun and Zhou [15] and Harnach and Niemann [20]. It is observed that the curves of the pressure pattern can be broadly divided into three regions: area I, area II, and area III. In area I ($0° \leq \theta < 40°$), the pressure is positive and more or less independent of the height z; in particular, at stagnation
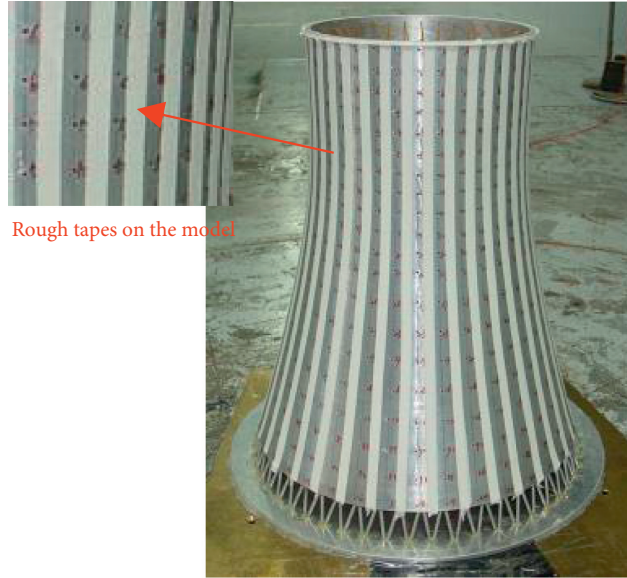
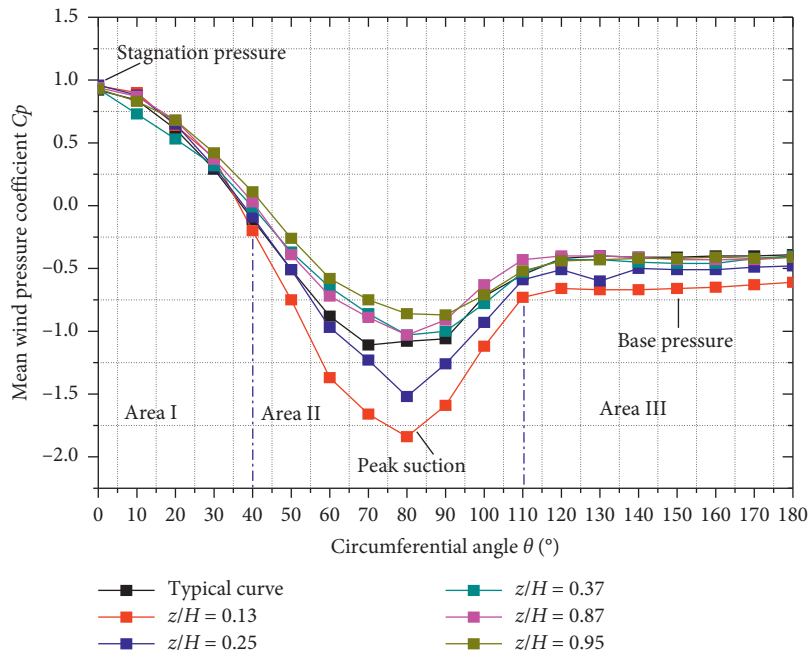FIGURE 4: Roughness simulation of the cooling tower surface.

FIGURE 5: Mean pressure coefficients at typical height.

($\theta = 0°$), the coefficient is still approximately unity. In area II ($40° < \theta < 110°$), the variation of the pressure coefficient with height is obvious. In particular, the typical and sensitive measure of the pressure distribution suction peak min Cp varies from -1.84 at $z/H = 0.13$ to -1.08 at $z/H = 0.95$. In area III ($110° < \theta < 180°$), since the flow separates from the sides of the body ($\theta = 110°$), the base pressure coefficient Cp,b is negative and independent of the circumferential angle θ. In addition, the variation of the base pressure coefficient Cp,b with height is small, apart from an area near the tower bottom, due to the flow separating from the lower edge of the shell.

Figure 6 shows typical parameters of the pressure distribution varying with height, where the pressure rise coefficient ΔCp representing the pressure rises downstream of the suction peak, min Cp, to the base pressure coefficient Cp,b at a horizontal level, is given by

$$\Delta Cp = \frac{Pb(z) - \min P(z)}{q(z)} = Cp, b(z) - \min Cp(z), \quad (3)$$

where $Pb(z)$ and min $P(z)$ are the base pressure and minimum pressure at height z, respectively.

From Figure 5, it is clear that the typical parameters of the pressure distribution in the lower third of the shell are
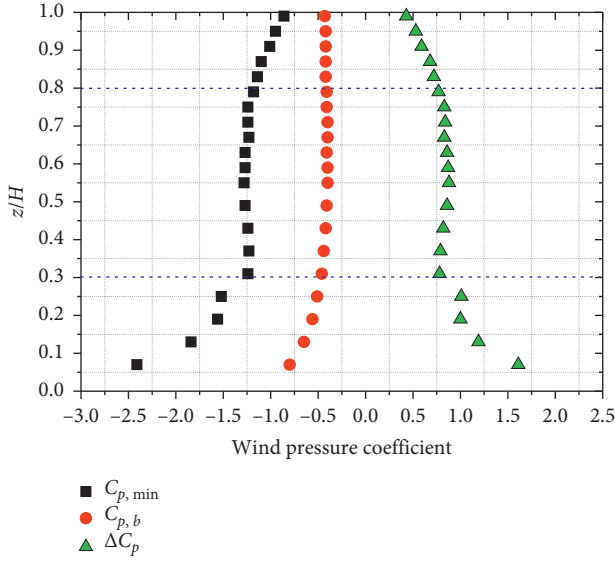
Figure 6: Characteristic value of pressure coefficients varying with height.

Figure 7: Aerodynamic coefficients at each section.

closely related to the height z. The suction peak min Cp varies from -2.41 to -1.24 over the region $z/H = 0.07$ to 0.31. Simultaneously, the base pressure Cp,b increases from -0.80 to -0.46. In an area near the upper tower, the suction peak min Cp varies from -1.18 at $z/H = 0.80$ to -0.86 at the top of the tower. However, due to the fact that the flow separates from the upper edge and from the sides of the shell, constant pressure is enforced on the wake region and the base pressure Cp,b is constant with respect to the height z by a pressure coefficient of -0.42. This is very close to the figure -0.39 reported by Harnach and Niemann [20]. In the region $z/H = 0.30$ to 0.80, the typical parameters are approximately constant with respect to the height z, resulting in an average min Cp and base pressure Cp,b of -1.25 and -0.42, respectively.

Pressure represents the local load acting on the surface of the shell; however, global forces such as resistance should also be considered in the design. For structures with circular cross sections, such as a cooling tower, the mean drag coefficient C_D in the downwind direction and lift coefficient C_L of a section obtained by the area-weighted integral of the mean pressure distributions are given by

$$C_D = \frac{\pi}{N} \sum_{i=1}^{N} \cos \theta_i \cdot Cp_i,$$

$$C_L = \frac{\pi}{N} \sum_{i=1}^{N} \sin \theta_i \cdot Cp_i,$$

(4)

where N is the number of pressure taps arranged uniformly in the circumferential direction and Cp_i and θ_i represent the pressure coefficient and circumferential angle at point i, respectively.

Figure 7 shows the result of the aerodynamic coefficients at each section. It can be seen that the average value of the lift coefficient C_L is basically constant along the height and is
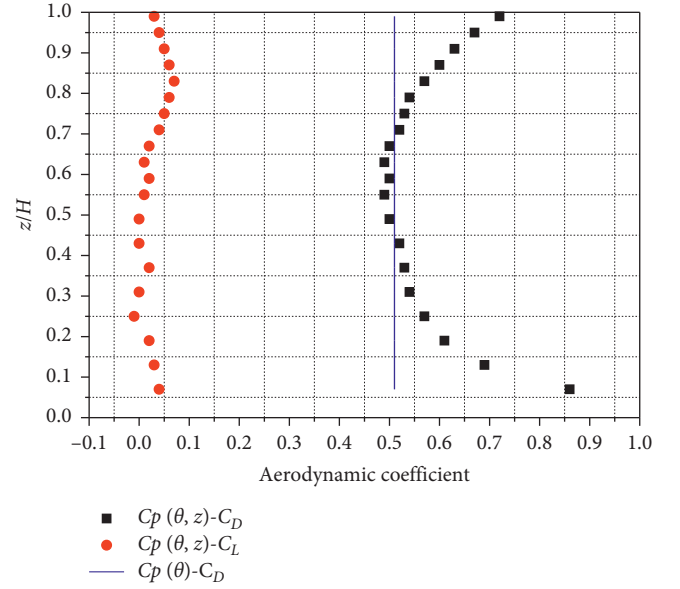
mostly close to zero. In fact, for the circular cross-section structure of the cooling tower, due to the symmetrical distribution of the wind pressure on the surface, the theoretical average value of the lift coefficient is zero. The consistency of the theoretical values verifies the correctness of the test results in the present study. The three-dimensional effect of the drag coefficient C_D is significant, showing the characteristics of a large end and a small middle. The drag coefficient at the top of the tower ($C_D = 0.72$) is 41.2% larger than the middle section, and the drag coefficient at the bottom of the tower ($C_D = 0.90$) is 76.5% larger than the middle section. It can be seen that if the design load is taken according to the "representative curve," the design load at both ends of the cooling tower will be significantly smaller than the actual load at the ends.

3. Effect of External Pressure on Wind-Induced Responses

3.1. Details of the Numerical Calculation. The numerical calculations of the wind-induced static response of the prototype cooling tower were carried out with the help of the finite element software ANSYS. The internal forces were calculated using the membrane theory of shells. The body of the tower was simulated using a SHELL63 element with four nodes and both membrane and flexural stiffnesses, and the columns were idealized as three-dimensional Timoshenko beams with a BEAM188 element. The finite element model and analysis result of the first-order modal are shown in Figure 8. The fundamental frequency f is 0.738 Hz, and there are 4 circular waves and 2 vertical waves in the mode.

The combined effects of the dead load g, the wind load acting on the external surface of the shell Pe, and the internal suction Pi were considered. They usually produce extreme stresses in the tower. For the wind load, a velocity pressure of $q(z) = q_{(10)} * (z/10)^{2\alpha} = 0.45(z/10)^{0.32}$ is applied, where q kN/
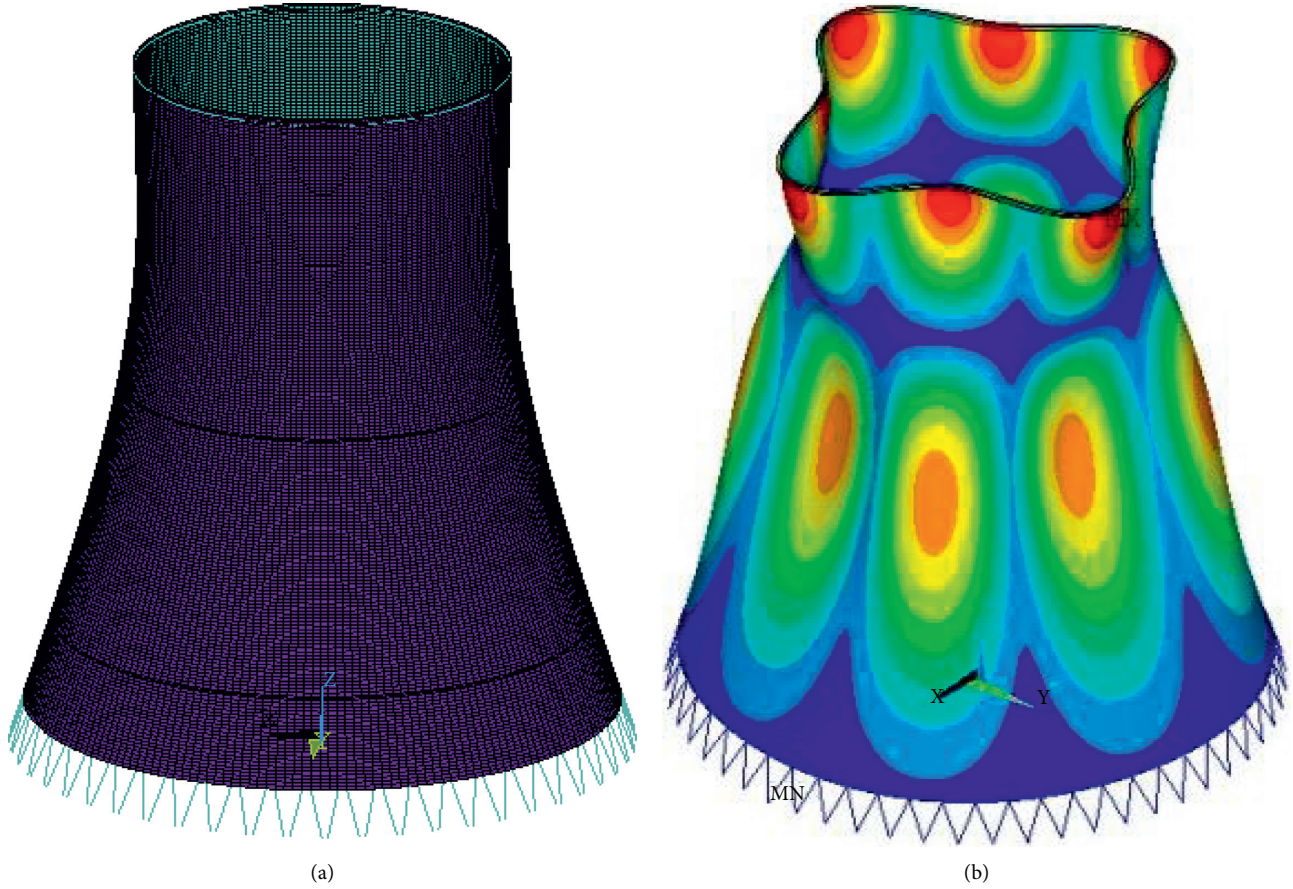
(a)

(b)

Figure 8: Finite element model and first-order modal. (a) Finite element model. (b) First-order modal ($f = 0.808$ Hz).

m^2 and z m, $\alpha = 0.16$ is the dimensionless power exponent, and $q_{(10)} = 0.45$ kPa. As mentioned before, two different pressure coefficients were investigated, that is, the simplified height-constant pressure coefficient $Cp(\theta)$ and the realistic pressure $Cp(\theta, z)$. Hence, two different wind loads acting on the external surface of the shell are given by

$$Pe, \text{simple} = Cp(\theta) \times q(z), \quad (5)$$

$$Pe, \text{realistic} = Cp(\theta, z) \times q(z). \quad (6)$$

In addition to the external surface, the internal surface of the cooling tower also suffers wind load due to allowing wind to pass through to the circulating cooling water. Since no regulations concerning the internal suction of the cooling towers have been included in the existing Chinese code, the value adopted in the present study is incorporated in the German code (VGB [21]). The internal suction Pi is constant with respect to the height z and the circumferential angle θ and related to the velocity pressure $q(H)$ at the top of the tower by a pressure coefficient of -0.50.

The buckling safety of the shell is one of the essential factors considered in the design of cooling towers. The Chinese codes have provided stability checking formulas for the entire cooling tower and the tower body, respectively. They are

$$q_{cr} = 0.052E\left(\frac{h}{r_0}\right)^{2.3}, \quad (7)$$

$$0.8K_B\left(\frac{\sigma_1}{\sigma_{cr1}} + \frac{\sigma_2}{\sigma_{cr2}}\right) + 0.2K_B^2\left[\left(\frac{\sigma_1}{\sigma_{cr1}}\right)^2 + \left(\frac{\sigma_2}{\sigma_{cr2}}\right)^2\right] = 1, \quad (8)$$

where q_{cr} is the critical wind pressure; E is the elasticity modulus of concrete; h is the wall thickness at the throat of the cooling tower; r_0 is the diameter at the throat; K_B is the safety factor for elastic buckling; σ_1 and σ_2 refer to the circumferential and meridian pressures, respectively; γ is the Poisson ratio of concrete; K_1 and K_2 are the parameters determined from the geometric parameters of the tower body; σ_{cr1} and σ_{cr2} are the critical circumferential and meridian pressures, respectively, which are given by

$$\sigma_{cr1} = \frac{0.985E}{\sqrt[4]{(1-\gamma^2)^3}}\left(\frac{h}{r_0}\right)^{4/3}K_1,$$

$$\quad (9)$$

$$\sigma_{cr2} = \frac{0.612E}{\sqrt[4]{(1-\gamma^2)^3}}\left(\frac{h}{r_0}\right)^{4/3}K_2.$$

$$V_{cr} = 40\sqrt{q_{cr}}. \quad (10)$$

According to equation (5), the unstable critical wind speed V_{cr} is calculated by

The critical circumferential and meridian pressures, σ_{cr1} and σ_{cr2}, can be calculated by equations (7) and (8), respectively. Substituting the hoop and meridional stresses calculated from ANSYS into equation (6), the safety coefficient of the local stability K_B can be obtained.

4. Results and Analysis of Static Responses

Since the maximum positive value (tension) of the membrane forces caused by wind load and dead load is usually at the windward meridian (0° meridian) and their maximum negative value (compression) is usually at about the 70° meridian, the membrane forces at the 0° and 70° meridian were taken as examples to analyze the influence of the pressure distribution on the static response of the cooling tower in this study. The membrane forces induced by the combined effects mentioned before are plotted in Figure 9. From Figure 9(a), it is observed that the simplified height-constant pressure distribution $Cp(\theta)$ results in considerably higher meridional axial forces compared to the realistic pressure distribution $Cp(\theta, z)$. The increase averaged over the height of the shell is about 20%. However, as seen in Figure 7, the overall aerodynamic drag of the realistic pressure distribution (the average value over the height is 0.61) is higher than the simplified (0.51). This is because cooling towers, like spatial structures in general, are sensitive not only to load intensity but just as much to the load distributions, which will be further explained in another section below. However, the pressure distributions exert little influence on the maximum tensile and compressive hoop axial force, as can be seen in Figure 9(b). The realistic pressure distribution produces slightly higher hoop axial forces in the lower third of the shell but smaller ones in the upper fifth of the shell. This is because the hoop forces are created mainly by the local effect of wind pressure at a given level, and the peak suctions of the realistic pressure distribution at the lower third and upper fifth of the shell are larger than those in the simplified pressure distribution. This is in accordance with the results reported by Harnach and Niemann [20]. Figures 9(c) and 9(d) show the comparison of the calculation results of the bending moments. It can be seen that the meridian and hoop bending moments under the two loads are basically the same along the height change trend, and the magnitudes are similar.

Figure 10 shows the comparison of the absolute value of the displacement under two wind pressure distribution curves. It can be seen that the trend of the deformation of the cooling tower is basically the same. The maximum deformation occurs near the throat, and the displacement under the action of the "sexual curve $Cp(\theta)$" is significantly larger (up to 15%) than that of the three-dimensional curve $Cp(\theta, z)$ at the height above 1/3 H. However, at the height below 1/3 H, the displacement under $Cp(\theta)$ is slightly smaller than that of $Cp(\theta, z)$. In order to observe the difference between the internal forces under the two loads more clearly, the meridian stress along the hoop direction at the typical upper, middle, and lower height sections of the cooling tower is displayed in Figure 11. It can be seen that the meridian stress under different loads has the same distribution trend along the hoop direction, and the stress peak value of the "representative curve $Cp(\theta)$" is slightly larger than that of the three-dimensional curve $Cp(\theta, z)$.

Table 1 shows the comparison of the maximum response and the occurrence location under the two wind loads. It can be seen from the table that the maximum response location under the two loads is basically the same, and the maximum displacement of the "representative curve $Cp(\theta)$" is slightly larger than that of the three-dimensional curve $Cp(\theta, z)$. The maximum principal tensile stress is quite different from the maximum principal compressive stress. The maximum principal tensile stress of the "representative curve" is 52% larger than that of the three-dimensional curve, and the absolute value of the maximum principal compressive stress is 52.7% smaller.

The buckling safety is tabulated in Table 2. Comparing the simplified height-constant pressure distribution $Cp(\theta)$ and the realistic pressure distribution $Cp(\theta, z)$, it can be seen that the buckling safety is generally smaller in the first case (the difference is 6.1%). In other words, with relation to buckling safety, the simplified approach $Cp(\theta)$ is always conservative. This also means that when determining the shell thickness for a given minimum buckling safety, the required wall thickness will be somewhat reduced when the realistic pressure distribution $Cp(\theta, z)$ is taken into account. In general, the effect of the pressure distribution on the buckling mode is slight.

5. Influence Mechanism of External Pressure on Wind-Induced Responses

5.1. Wind Pressure Curves Detailed by the Specifications. The current relevant design codes for cooling tower design in China respectively give two average wind pressure coefficient distribution curves for smooth and ribbed hyperbolic cooling towers, and the expression adopts the Fourier series as listed in equation (11) (GB/T 50102, 2003; NDGJ5-88, 2006). The German standard gives 6 curves according to the surface roughness and uses the piecewise function expression (VGB, 2010), but Gould and Kratzig [22] pointed out that the German curve can also be expressed by the Fourier series polynomials for design input. Therefore, the least squares method is adopted to fit the German code curves into an eight-term Fourier series in the present study, which unifies the expression form of the Chinese and German gauge curves. The comparison between the Chinese and German standard curves and the harmonic coefficients of each order is shown in Figure 12 and Table 3.

$$C_p(\theta) = \sum_{i=0}^{7} a_i \cos(i * \theta), \quad (11)$$

where a_i is the ith harmonic coefficient; θ is the angle with the incoming flow direction.

Taking VGB-K1.0 as an example, the comparison of the wind pressure coefficients of the various harmonic components is depicted in Figure 13. It can be seen that a_0 is the
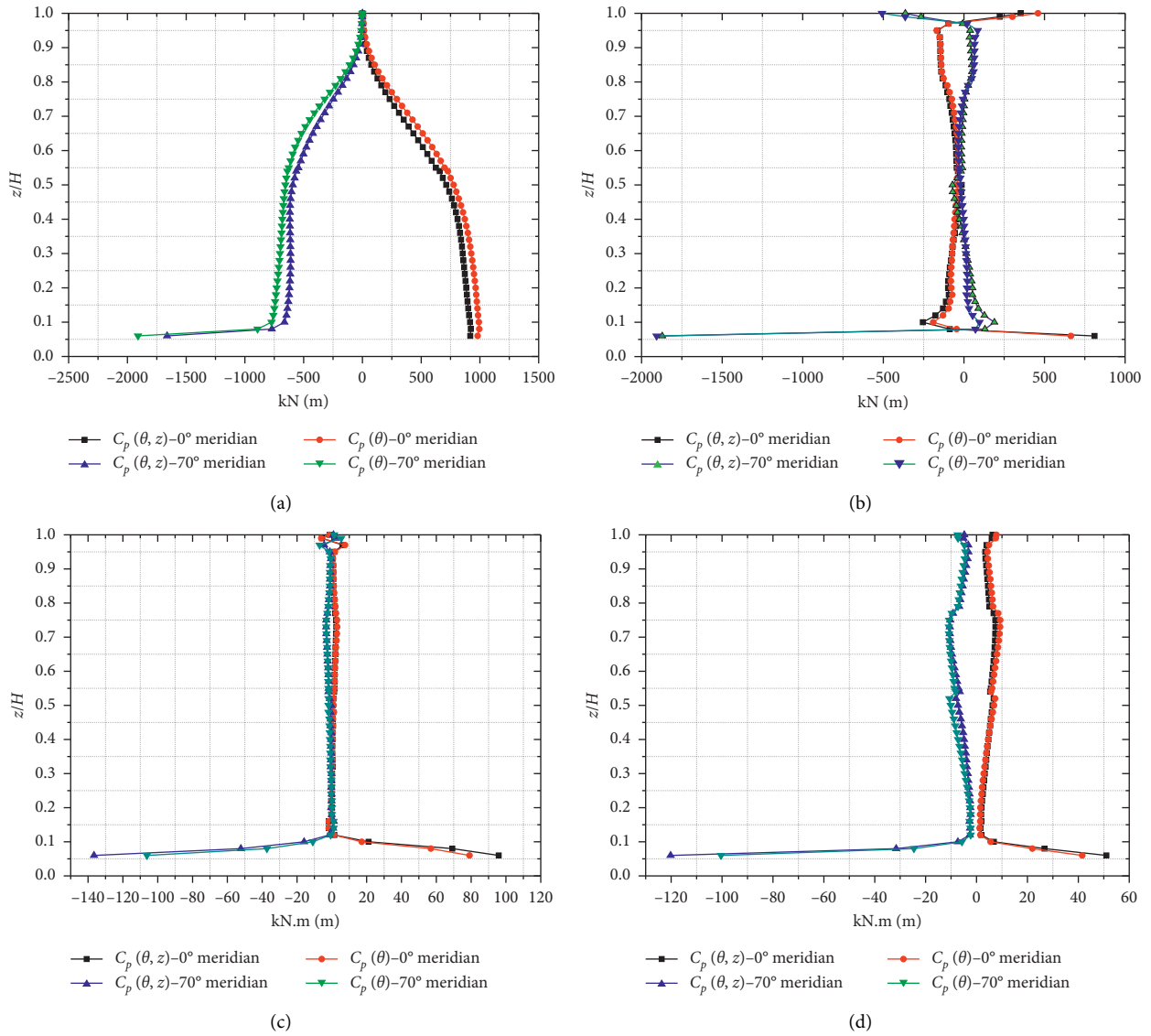
Figure 9: Comparison of membrane forces. (a) Meridional axial force. (b) Hoop axial force. (c) Meridional bending moment. (d) Hoop bending moment.
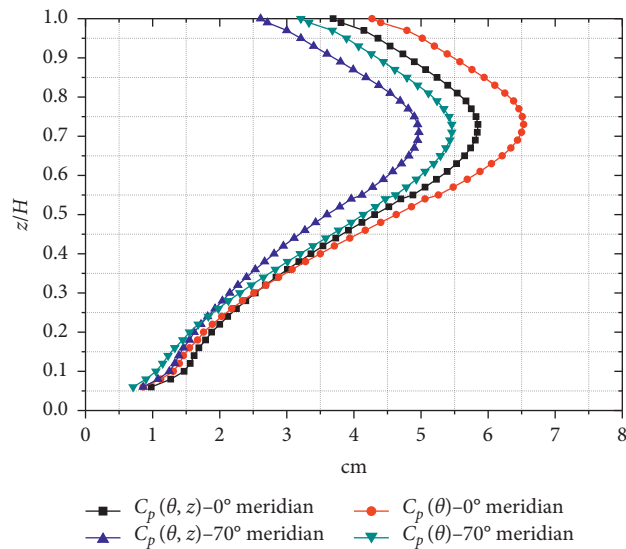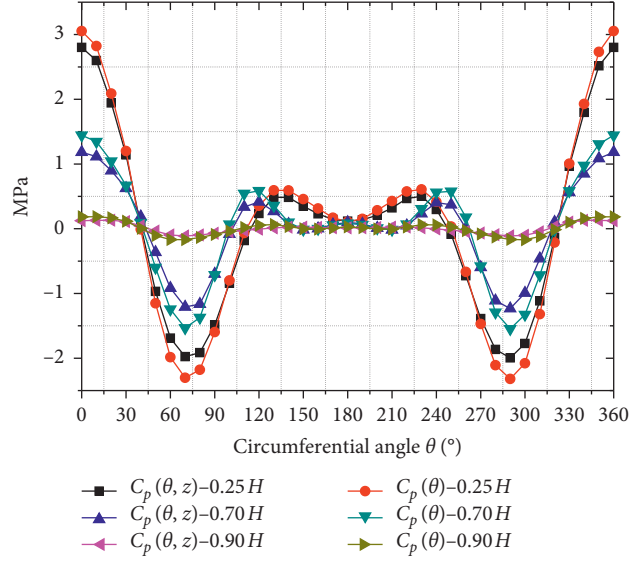

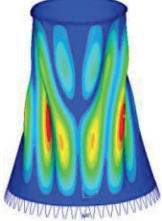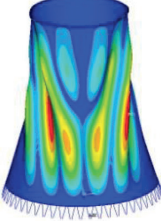Figure 10: Comparison of displacement.

Figure 11: Comparison of meridional stress at typical height.

Table 1: Comparison of max response.

Pressure coefficient	Max displacement			Max principal tensile stress			Max principal compressive stress		
	θ (°)	z/H	Disp. (m)	θ (°)	z/H	Stress (MPa)	θ (°)	z/H	Stress (MPa)
$Cp(\theta)$	0	0.74	0.065	0	0.21	3.13	±69	0.19	−2.47
$Cp(\theta, z)$	0	0.72	0.060	0	0.18	2.06	±73	0.17	−5.22

Table 2: Comparison of overall buckling.

Method	Equation (7)	ANSYS	
Pressure coefficient	—	$Cp(\theta, z)$	$Cp(\theta)$
V_{cr}	123.78 m/s	119.56 m/s	112.68 m/s
Buckling mode	—		

direct current component, which is equivalent to the uniform pressure acting in the radial direction of the cooling tower. Since a_0 is a negative value, its effect is expressed as suction. a_i is the wind pressure coefficient of the i-th harmonic. The wind pressure coefficient of the 7th harmonic fluctuates near zero, and its shape is approximately a straight line because the coefficient a_7 is small. The sum of those terms is the VGB-K1.0 wind pressure curve.

Table 4 shows the comparison between the downwind drag coefficient and the total drag coefficient obtained by integrating the corresponding wind pressure coefficients of each harmonic component of the specification curve along the circumference. It can be seen from the table that the downwind drag coefficient is completely contributed by the wind pressure coefficient of the first harmonic, and the wind pressure coefficients of other harmonics contribute zero to

the total drag coefficient. In fact, from the calculation expression of the harmonic resistance coefficient of each order (equation (11)), only when $i = 1$, Cd_i is not zero, so the total resistance $C_D = \sum Cd_i = Cd_1 = a_1\pi/2$.

$$Cd_i = 0.5 \int_0^{2\pi} a_i \cos(i * \theta)\cos(\theta)d\theta = \begin{cases} i = 1 & Cd_i = \dfrac{a_i\pi}{2} \\ \\ i \neq 1 & Cd_i = 0 \end{cases}.$$

(12)

From the analysis of the contribution of each order of harmonics to the drag coefficient, it can be seen that the DC component a_0, which is probably equal around the surface, induces the uniform expansion of the circular section without rigid body displacement; that is, the drag coefficient
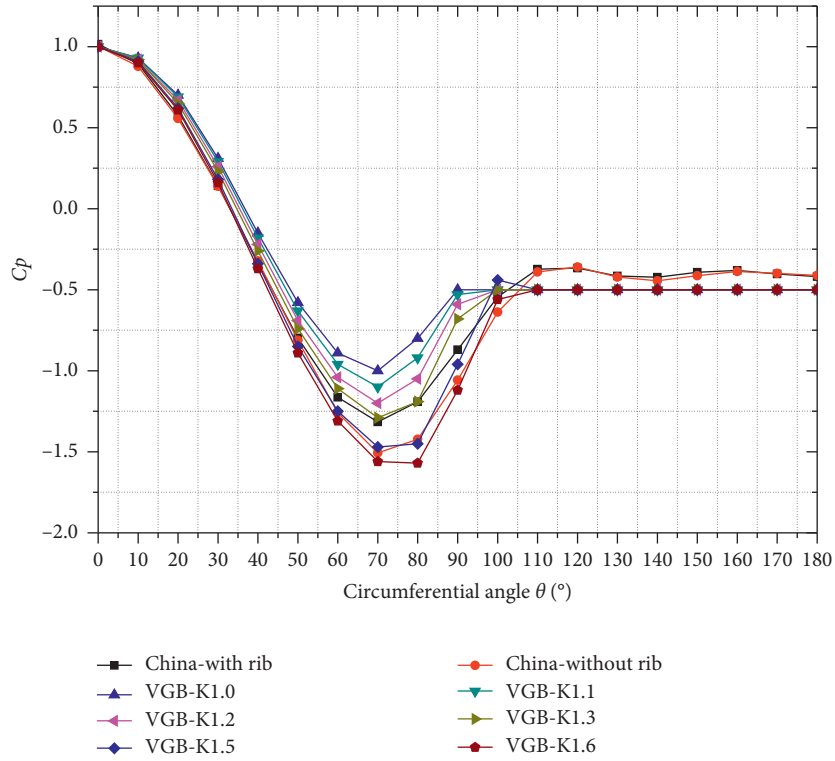
Figure 12: Wind pressure coefficient in China and German codes.

Table 3: The Fourier coefficients of each harmonic of specification curves.

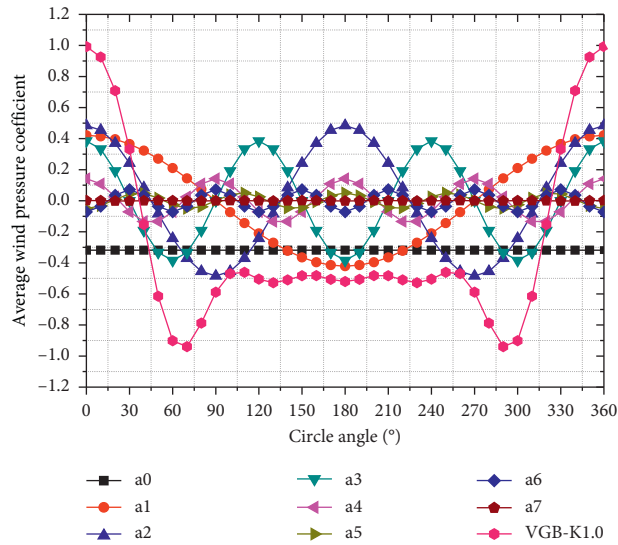| Specification curve	Harmonic coefficient							
	a_0	a_1	a_2	a_3	a_4	a_5	a_6	a_7
China-with rib	−0.3919	0.2581	0.6013	0.5042	0.1052	−0.0955	−0.0194	0.0475
China-without rib	−0.4425	0.2460	0.6757	0.5356	0.0609	−0.1393	0.0010	0.0644
VGB-K1.0	−0.3181	0.4211	0.4841	0.3844	0.1419	−0.0506	−0.0718	0.0014
VGB-K1.1	−0.3421	0.4018	0.5106	0.4142	0.1394	−0.0687	−0.0736	0.0137
VGB-K1.2	−0.3715	0.3773	0.5397	0.4459	0.1351	−0.0861	−0.0714	0.0269
VGB-K1.3	−0.4012	0.3549	0.5723	0.4756	0.1256	−0.1029	−0.0630	0.0419
VGB-K1.5	−0.4616	0.3096	0.6408	0.5378	0.1021	−0.1412	−0.0421	0.0730
VGB-K1.6	−0.4994	0.2937	0.6938	0.5559	0.0711	−0.1467	−0.0200	0.0714

Figure 13: Pressure curves of each harmonic component (VGB-K1.0).

TABLE 4: Cd of each harmonic component.

Specification curve	Drag coefficient of each harmonic component								C_D
	$Cd\text{-}a_0$	$Cd\text{-}a_1$	$Cd\text{-}a_2$	$Cd\text{-}a_3$	$Cd\text{-}a_4$	$Cd\text{-}a_5$	$Cd\text{-}a_6$	$Cd\text{-}a_7$	
China-with rib	0.00	0.41	0.00	0.00	0.00	0.00	0.00	0.00	0.41
China-without rib	0.00	0.39	0.00	0.00	0.00	0.00	0.00	0.00	0.39
VGB-K1.0	0.00	0.66	0.00	0.00	0.00	0.00	0.00	0.00	0.66
VGB-K1.1	0.00	0.64	0.00	0.00	0.00	0.00	0.00	0.00	0.64
VGB-K1.2	0.00	0.60	0.00	0.00	0.00	0.00	0.00	0.00	0.60
VGB-K1.3	0.00	0.56	0.00	0.00	0.00	0.00	0.00	0.00	0.56
VGB-K1.5	0.00	0.49	0.00	0.00	0.00	0.00	0.00	0.00	0.49
VGB-K1.6	0.00	0.46	0.00	0.00	0.00	0.00	0.00	0.00	0.46
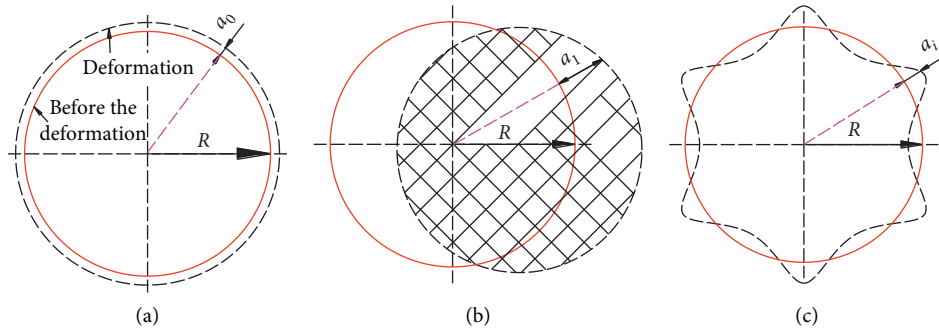
FIGURE 14: Radial displacement of each harmonic component. (a) a_0. (b) a_1. (c) a_i ($i = 2$–7).

of a_0 is zero. The first-order component a_1, which may be a superposition of uniform force around the surface and a whole deflection force acting on the structure, causes rigid body displacement of the cooling tower without local deformation of the circular section; that is, the drag coefficient of a_1 is equal to the drag of the entire wind pressure curve zero. The higher-order component a_2~a_7, which is not a uniform force around the surface, induces localized deformation in the circular section, but no rigid body displacement; that is, the drag coefficient of a_2~a_7 is zero. A schematic diagram of the radial displacement component generated by each order of harmonics is shown in Figure 14. It can be seen that the contribution of the order of harmonics is shown in Figure 14. The cross-sectional resistance coefficient of the cooling tower to the overall displacement of the structure is only the rigid body displacement.

5.2. Influence of Different Wind Pressure Curves on the Response of Cooling Tower. Taking the finite element model in Figure 8 as an example, the wind pressure curves specified in Figure 12 are adopted to study the influence of different wind pressure curves on the response of the cooling tower. Because the meridian stress and other response results are basically consistent with the change law of the displacement response, the present study only analyzes the wind-induced displacement response.

Figure 15 shows the calculation results of the displacement response at the throat of the harmonic components of each order of the Chinese ribbed curve. It can be seen that the distribution of the displacement components generated by the harmonics of each order is consistent with the analysis conclusion of Figure 14; that is, the DC

component induces the uniform expansion of the circular section, the first-order component causes the rigid body displacement of the cooling tower, and the higher-order component causes the local deformation of the circular section. The inference of Figure 15 is further confirmed.

The displacement of each harmonic component at the meridian of 0° (maximum positive pressure zone) and 70° (minimum negative pressure zone) is shown in Figure 16. It can be found from Figure 16(a) that the displacement of the first-order harmonic component of each standard curve increases along the height, and the displacement of the same height increases with the increase of the drag coefficient C_D of the standard curve. This is because the effect of the first-order harmonic is resistance. The cooling tower structure undergoes a deformation similar to that of a vertical cantilever beam under the action of this component. The deformation size increases with heights; the greater the resistance, the greater the deflection induced. It can be seen from Figure 16(b) that the displacement caused by the DC and high-order harmonic components shows a distribution trend that is large near the throat and small at both ends along the height. This phenomenon can be explained as the effect of DC and high-order harmonic components. The results show that the shell is locally deformed and the deformation is related to the local stiffness of the shell. The bottom is the area with the largest cooling tower wall thickness, so the stiffness of this area is the largest in the structure. The middle section is the thinnest part of the cooling tower wall, so its rigidity is the smallest. Although the top wall is thinner and the size is the same as the middle section, the rigid ring on the top greatly enhances the rigidity of the area. Therefore, it is not difficult to understand that the
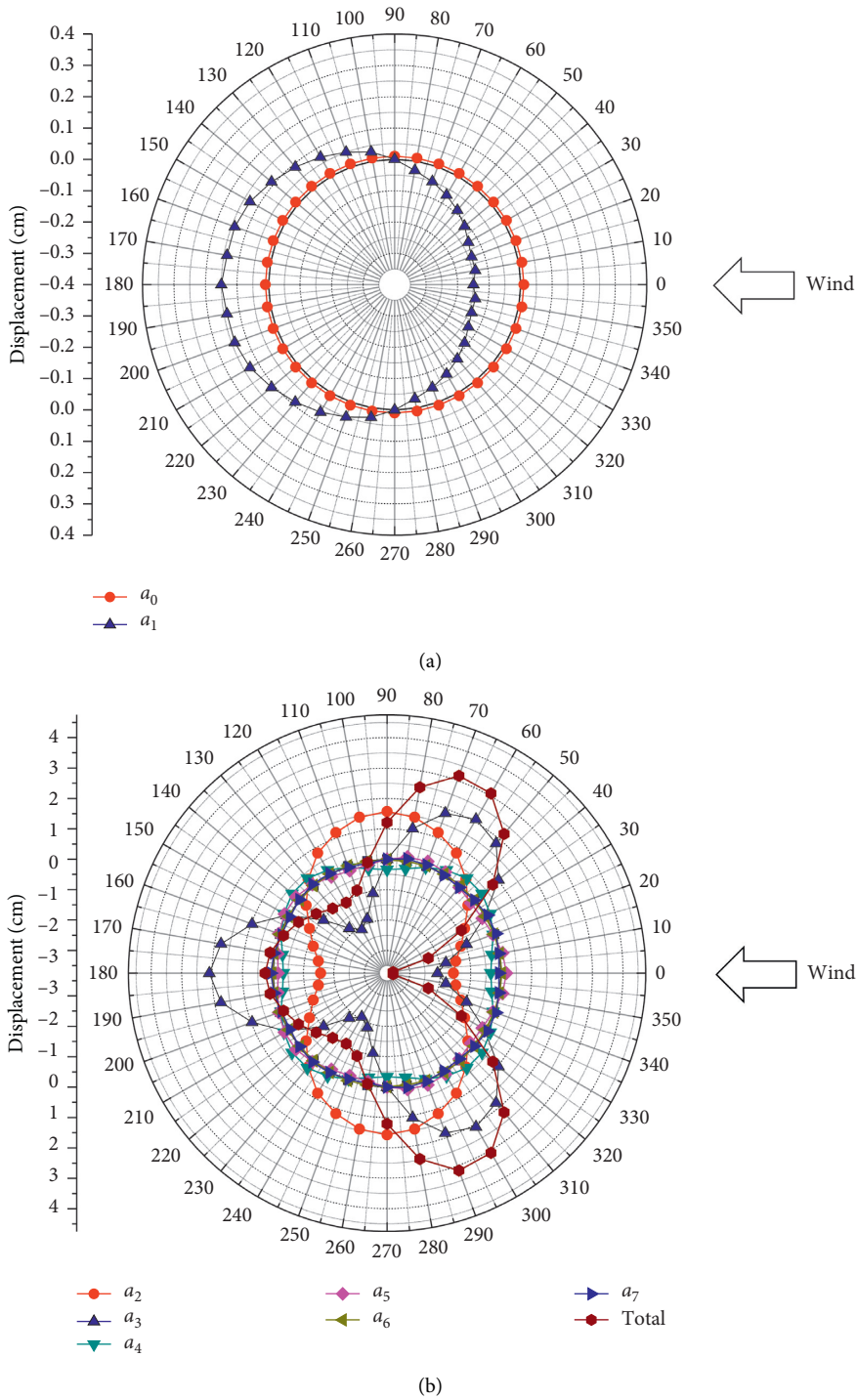
(a)

(b)

FIGURE 15: Radial displacement of each harmonic component for rib curve in China code (throat). (a) Displacement of DC and first-order harmonic component. (b) High-order harmonic component displacement and total displacement.

local deformation of the shell occurs near the throat. The displacement of the DC and higher-order harmonic components at the same height decreases with the increase of the resistance coefficient of the gauge curve. This is because the local deformation of the shell is more closely related to the local wind pressure. In fact, as the drag coefficient C_D of the wind pressure curve increases, the minimum wind pressure coefficient amplitude decreases, and the maximum local load decreases, so the local deformation of the shell also decreases. The distribution law of the overall displacement is basically consistent with the displacement of the DC and high-order harmonic components (Figure 16(c)), indicating
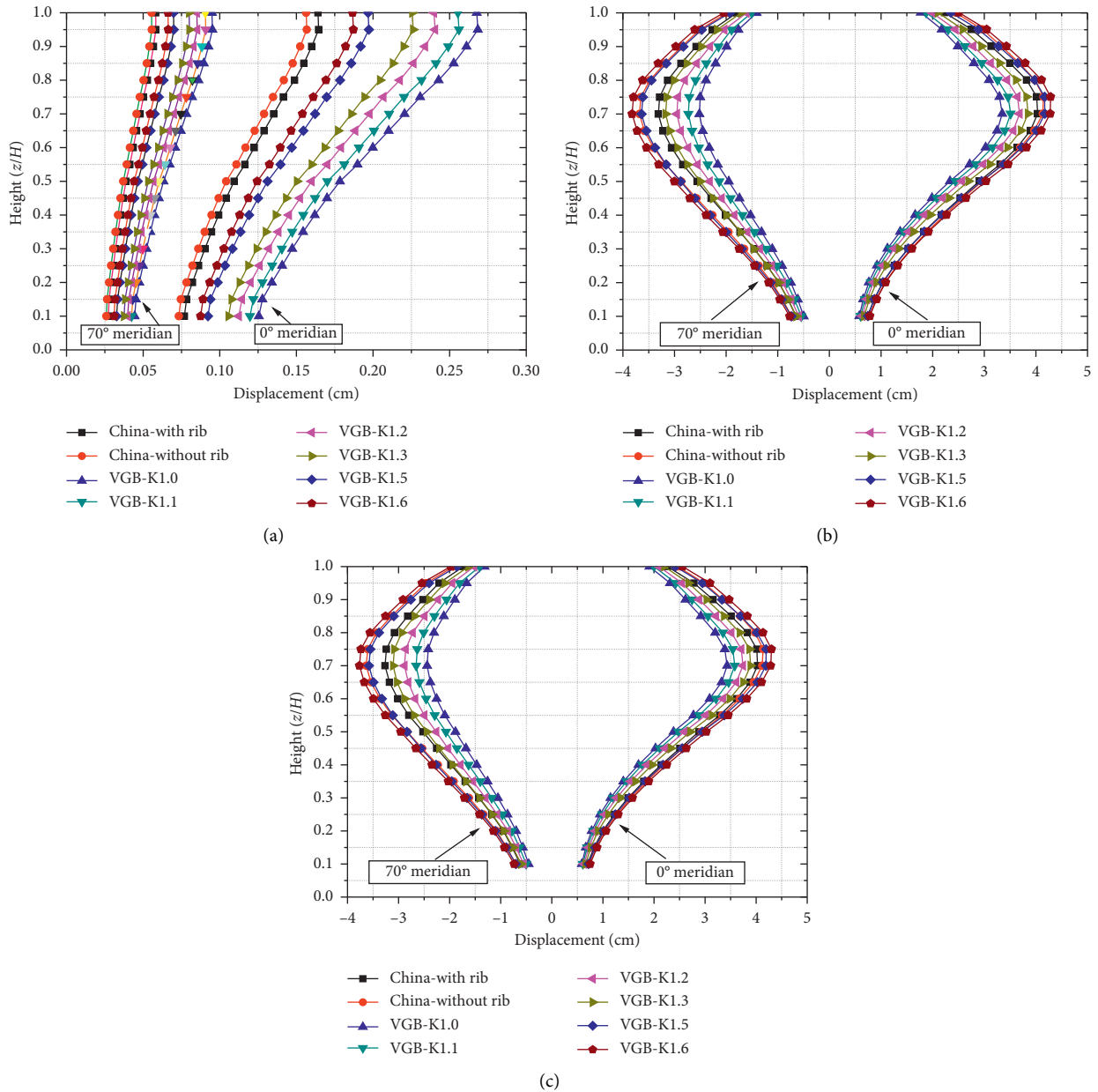
(a)

(b)

(c)

FIGURE 16: Total displacement and component for each component. (a) Displacement of the first-order harmonic component. (b) Displacement of DC and high-order harmonic components. (c) Total displacement.

that the wind-induced deformation of the cooling tower is dominated by the local deformation of the shell.

Figure 17 shows the $0°$ and $70°$ meridian displacement of the first-order harmonic component as a percentage of the total displacement. It can be seen that the displacement ratio of the first-order harmonic component is mostly below 10%, which increases slightly as the resistance increases. Contrary to the distribution trend of the total displacement, the proportion of the first-order harmonic component changes along the height following a trend wherein it is small in the middle and large at both ends.

Figure 18 shows the comparison of the displacement percentage of the harmonic components of each order of the standard curves. It can be seen that the displacement

percentages of the harmonic components of each order of the different standard curves are basically the same. The third-order harmonic has the largest proportion, which is about 55%, followed by the second-order harmonic (about 35%), while the first-order harmonic is only about 5%.

It can be clearly seen from Figure 19 that the displacement of the first-order harmonic component increases with the increase of the resistance, but its largest proportion of the total displacement is only 7%. In spite of the fact that the displacement of the DC and higher-order harmonic components decreases with the increase of the drag coefficient C_D, its minimum proportion is still above 93%. The "increase" is much smaller than the "decrease," so the total displacement decreases as the drag coefficient increases.
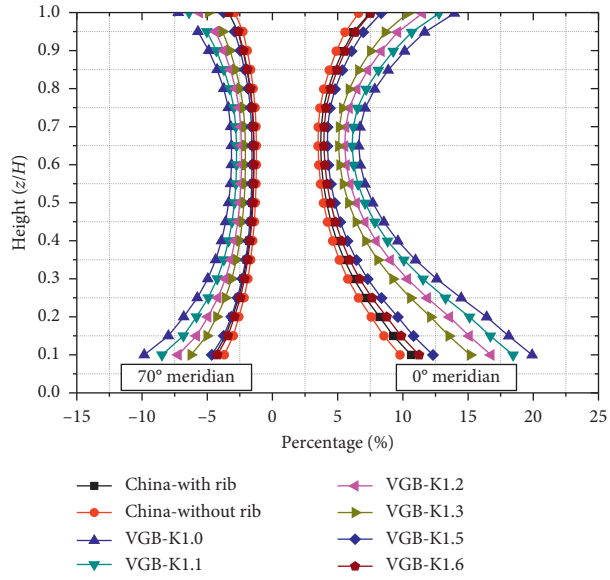
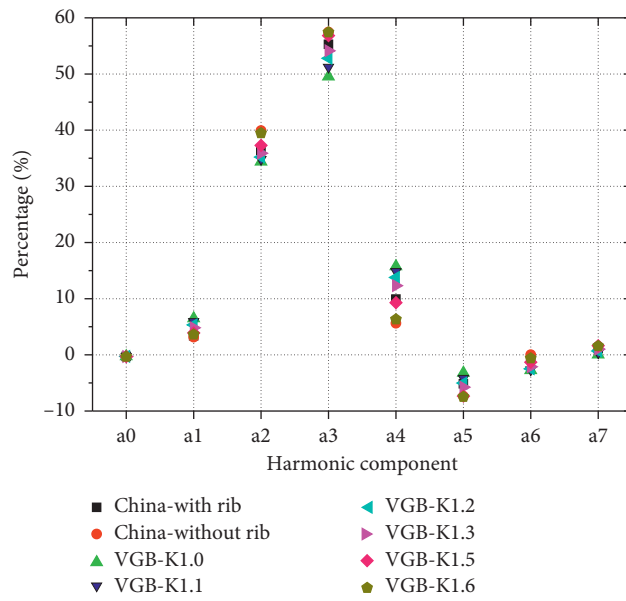Figure 17: Percentage of first-order harmonic displacement.

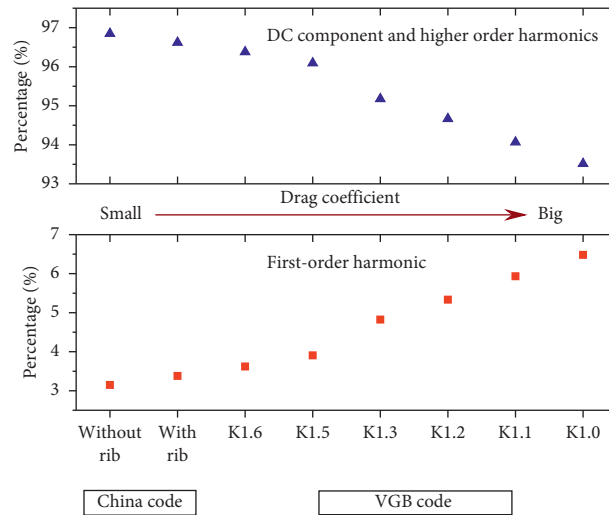Figure 18: Percentage of each harmonic displacement (middle average).

FIGURE 19: Percentage of first-order and high-order harmonic displacement (middle average).

6. Conclusions

Based on rigid model pressure measurement wind tunnel tests, the three-dimensional wind pressure coefficient distribution curve $C_p(z, \theta)$ of a 200 m high super large cooling tower in a nuclear power plant was obtained along the height and circumferential direction. The three-dimensional effect of the wind load on the outer surface of the cooling tower was analyzed. The static response and the buckling safety under the three-dimensional wind pressure coefficient curve $C_p(z, \theta)$ and the "representative curve $C_p(\theta)$" were then calculated, and the influence mechanism of the external pressure on the wind-induced response was analyzed. The following main conclusions were drawn:

(1) The wind pressure coefficient on the outer surface of the cooling tower is basically symmetrically distributed along the circumferential direction, and the average value of the lift coefficient is close to zero. The three-dimensional effect of the wind pressure distribution makes the three-dimensional effect of the drag coefficient significant. Besides, the drag coefficient is characterized by a large value at the end of the cooling tower and a small value at the middle of the cooling tower. The drag coefficients at both ends are greater than that of the middle section.

(2) The wind-induced response of the cooling tower is dominated by the local shell deformation. The rigid deformation caused by resistance does not exceed 10% of the total response, while the local shell deformation caused by other harmonics accounts for more than 90% of the total response. The overall response of the cooling tower has no absolute relationship with the drag coefficient but is closely related to the characteristics of the wind pressure distribution.

(3) The coefficient distribution curve of the three-dimensional average wind pressure $C_p(z, \theta)$ along the height and the circumferential direction is simplified to the wind pressure distribution curve along the constant height $C_p(\theta)$. Although the overall wind load of the structure is underestimated, the wind-induced response of the cooling tower is more closely related to the distribution of the wind load. The response induced by the "representative curve $C_p(\theta)$" is basically the same as the three-dimensional curve $C_p(z, \theta)$, and the meridian internal force is even larger than the three-dimensional curve. In general, replacing the three-dimensional curve with the average curve of each height in the middle section is an effective simplification method that can meet the design requirements of the project.

Data Availability

The data used to support the findings of this study are available from the corresponding author upon request.

Conflicts of Interest

The authors declare that there are no conflicts of interest regarding the publication of this paper.

Acknowledgments

References

[1] P. C. Bamu and A. Zingoni, "Damage, deterioration and the long-term structural performance of cooling-tower shells: a survey of developments over the past 50 years," *Engineering Structures*, vol. 27, no. 12, pp. 1794–1800, 2005.

[2] H. J. Nimeann and W. Zerna, "Impact of research on development of large cooling towers," *Journal of Engineering Structures*, vol. 8, pp. 74–86, 1986.

[3] M. G. Hashish and S. H. Abu-Sitta, "Response of hyperbolic cooling towers to turbulent wind," *Journal of Structural Engineering*, vol. 100, no. ST5, pp. 1037–1051, 1974.

[4] J. Armitt, "Wind loading on cooling towers," *Journal of Structural Division*, vol. 106, no. ST3, pp. 623–641, 1980.

[5] CEGB, *Report of the Committee of Inquiry into the Collapse of Cooling Towers at Ferrybridge on November 7*, Central Electricity Generating Board, London, UK, 1965.

[6] Y. Zou, Z. Fu, X. He et al., "Characteristics of wind loading on internal surface and its effect on wind-induced response of a super-large natural-draught cooling tower," *Wind and Structures*, vol. 29, no. 4, pp. 235–246, 2019.

[7] S. T. Ke and Y. J. Ge, "The influence of self-excited forces on wind loads and wind effects for super-large cooling towers," *Journal of Wind Engineering and Industrial Aerodynamics*, vol. 132, pp. 125–135, 2014.

[8] S. Ke, H. Wang, and Y. Ge, "Interference effect and the working mechanism of wind loads in super-large cooling towers under typical four-tower arrangements," *Journal of Wind Engineering and Industrial Aerodynamics*, vol. 170, pp. 197–213, 2017.

[9] L. Zhao, Y. Ge, and A. Kareem, "Fluctuating wind pressure distribution around full-scale cooling towers," *Journal of Wind Engineering and Industrial Aerodynamics*, vol. 165, pp. 34–45, 2017.

[10] J.-F. Zhang, Y.-J. Ge, L. Zhao, and B. Zhu, "Wind induced dynamic responses on hyperbolic cooling tower shells and the equivalent static wind load," *Journal of Wind Engineering and Industrial Aerodynamics*, vol. 169, pp. 280–289, 2017.

[11] Y.-f. Zou, X.-h. He, H.-q. Jing, S. Zhou, H.-w. Niu, and Z.-q. Chen, "Characteristics of wind-induced displacement of super-large cooling tower based-on continuous medium model wind tunnel test," *Journal of Wind Engineering and Industrial Aerodynamics*, vol. 180, pp. 201–212, 2018.

[12] S. H. Abu-Sitta and M. G. Hashish, "Dynamic wind stresses in hyperbolic cooling towers," *Journal of the Structural Division*, vol. 99, no. 9, pp. 1823–1835, 1973.

[13] M. Kasperski and H.-J. Niemann, "On the correlation of dynamic wind loads and structural response of natural-draught cooling towers," *Journal of Wind Engineering and Industrial Aerodynamics*, vol. 30, no. 1–3, pp. 67–75, 1988.

[14] S. T. Ke, Y. J. Ge, L. Zhao, and Y. Tamura, "A new methodology for analysis of equivalent static wind loads on super-large cooling towers," *Journal of Wind Engineering and Industrial Aerodynamics*, vol. 111, pp. 30–39, 2012.

[15] T. F. Sun and L. M. Zhou, "Wind pressure distribution around a ribless hyperbolic cooling tower," *Journal of Wind Engineering and Industrial Aerodynamics*, vol. 54, no. 55, pp. 213–225, 1983.

[16] T. F. Sun, Z. F. Gu, L. M. Zhou, P. H. Li, and G. L. Cai, "Full-scale measurement and wind-tunnel testing of wind loading on two neighboring cooling towers," *Journal of Wind Engineering and Industrial Aerodynamics*, vol. 43, no. 1-3, pp. 2213–2224, 1992.

[17] China Planning Press, Ministry of Construction of the People's Republic of China, *GB/T 50102-2003, Code for Design of Cooling for Industrial Recalculating Water*, China Planning Press, Beijing, China, 2003, in Chinese.

[18] The people's Republic of China National Development and Reform Commission, *NDGJ5-88, Technical Specification for Hydraulic Design of Thermal Power Plant*, China Electric Power Press, Beijing, China, 2006, in Chinese.

[19] J. Emilia, B. Zdenek, and O. Fischer, "Vibration characteristics of a cooling-tower shell," *Journal of Wind Engineering and Industrial Aerodynamics*, vol. 12, pp. 145–154, 1983.

[20] R. Harnach and H.-J. Niemann, "The influence of realistic mean wind loads on the static response and the design of high cooling towers," *Engineering Structures*, vol. 2, no. 1, pp. 27–34, 1980.

[21] Bautechnik bei Kühltürmen-VGB PowerTech, *Structural Design of Cooling Tower- Technical Guideline for the Structural Design, Computation and Execution of Cooling Towers*, BTR Bautechnik bei Kühltürmen, Essen, Germany, 2010.

[22] P. L. Gould and W. B. Kratzig, *Cooling Tower Structures. Structural Engineering Handbook*, CRC Press LLC, Boca Raton, FL, USA, 1999.